SnT 2021
CTBT: SCIENCE AND TECHNOLOGY CONFERENCE

CTBTO
PREPARATORY COMMISSION

Infrasound propagation using atmospheric fields from high-resolution global models resolving gravity waves

C. Listowski[1], C. Stephan[2], A. Le Pichon[1], A. Hauchecorne[3], U. Achatz[4], and G. Bölöni[4,*]

[poster P1.1-491]

[1]CEA/DAM/DIF, F-91297, Arpajon, France
[2]Max Planck Institute for Meteorology, Hamburg, Germany
[3]LATMOS/IPSL, UVSQ Université Paris-Saclay, Sorbonne Université, CNRS, Guyancourt, France
[4]Goethe-Universität Frankfurt, Frankfurt, Germany
*now at Deutscher Wetterdienst, Offenbach am Main, Germany

POSTER

Infrasound propagation simulations using atmospheric fields from high-resolution global models resolving gravity waves

C. Listowski et al.

ABSTRACT

Small-scale atmospheric perturbations known as gravity waves (GW) are critical to infrasound propagation simulations as they alter the propagation path of the waves, causing detections at infrasound stations that remain unexplained when only large scale atmospheric features are considered.

Several pathways have been explored in the infrasound community, e.g. parameterizations based on the GW universal spectrum (e.g. Gardner et al. 1993 as in Vallage et al. 2021), stochastic parameterizations accounting for the intermittency of the GW field (e.g. de la Camara et al., 2015 as in Cugnet et al. 2019), GW ray-tracing equations applied to a frequency spectrum (Drob et al. 2013) or 3D GW-spectrum model (Chunchuzov & Kulichkov, 2019). Other paths, like parameterization accounting for non-dissipative interactions between the mean field and the GW field (Bölöni et al. 2021 ; Kim et al. 2021) remain to be explored. Meanwhile, working with models explicitly resolving a large part of the GW spectrum is another approach, which deserves to be considered given increasing computing means made available by HPC facilities.

We use modelled atmospheric fields obtained in the framework of the Dynamics of the Atmospheric General Circulation Modeled on Nonhydrostatic Domains (DYAMOND) initiative (Stevens et al. 2019). This international project, initiated by the Max Planck Institute for Meteorology (MPIM) and the University of Tokyo, describes a framework for the intercomparison of high-resolution global atmospheric models. It mainly focuses on tropospheric weather, but some models were run with a high enough top so that GW are resolved up to the stratosphere.

DYAMOND outputs provide a tool to globally evaluate how GW affect infrasound propagation across the IMS. We investigate how different configurations of the Icosahedral Non-hydrostatic (ICON) model lead to different gravity wave characteristics at infrasound stations and derive gravity wave potential energy distribution across the IMS network. Rayleigh lidar observations made at Observatoire de Haute Provence (OHP) are used to validate the modelled mean/GW fields at this location. We discuss the possibility of quantifying how GW affect infrasound propagation, using a ray-tracing tool.

Infrasound propagation simulations using atmospheric fields from high-resolution global models resolving gravity waves

C. Listowski et al.

INTRODUCTION

- Gravity waves (GW) are critical to explain infrasound guiding in the middle atmosphere, hence for the analysis of signals of interest at IMS and national stations *(Drob et al., 2013 ; Hedlin and Drob, 2014 ; Le Pichon et al. 2019 ; Vallage et al. 2021)*

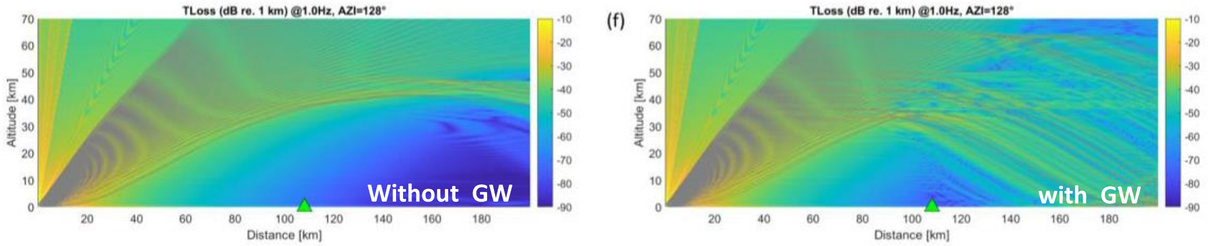

Attenuation (dB) of the acoustic energy (1 Hz) in one direction. Figures from the SI of Vallage et al. (2021)

- There are various sources of GW (orography, convection, fronts, jets, shears,…) and GW encounter propagation conditions that vary with season and location (*Fritts and Alexander, 2003, JGR*). Hence, infrasound detection at each IMS infrasound station is affected in different ways by GW activity.

- We are interested in assessing the impact of GW. For consistency, one needs to use a common tool to describe (at least a part of) the GW spectrum at the global scale.

- The DYAMOND initiative (https://www.esiwace.eu/services/dyamond) is mainly dedicated to atmospheric simulations at global scale and storm-resolving resolutions (< 5 km) in order to assess the performance of different model configurations and different models in capturing tropospheric weather and more particularly deep convection without parameterization *(Stevens et al. 2019).* GW are explicitly resolved and no GW parameterization is used.

- Model configurations of DYAMOND extend into the middle atmosphere, giving the opportunity to investigate GW momentum fluxes in the stratosphere *(Stephan et al. 2019, JAS ; Stephan et al. 2019, JGR).*

- Hence, we aim at characterizing gravity wave activity with these fields at the IMS stations and how these GW affect infrasound propagation simulations. This presentation shows preliminary results in this effort to assess the added value of such simulations for the infrasound community.

Infrasound propagation simulations using atmospheric fields from high-resolution global models resolving gravity waves

C. Listowski et al.

TOOLS

DYAMOND outputs (from an initiative led by MPIM and University of Tokyo)

We have used four configurations of the ICON model, so far.
ICON is the Icosahedral Nonhydrostatic Weather and Climate Model developped by DWD (German weather service) and MPIM (Zängl et al. 2014).

The period investigated corresponds to the second experimental phase (https://www.esiwace.eu/services/dyamond/winter).

Period: 20 Jan. 2020 – 29 Feb. 2020
Initialization and running mode : ECMWF/IFS ; freely-running
Horizontal resolution is : 5 km / Model top : 75 km
Fields considered here go up to 45 km altitude (Nlevels= 77), i.e. below the sponge layer (to avoid artificially damped fields).
The used outputs are regridded on a 0.35° x 0.35° grid (dx < 40 km)

Outputs (3-hourly) are named:
dpp0014: uncoupled (atmosphere/ocean) simulation
dpp0015: coupled simulation
dpp0016: coupled simulation ; increased ocean albedo
nwp2.5winter: NWP simulation with horizontal resolution of 2.5 km
(nwp2.5 and dpp00XX have different land scheme, turbulent scheme and different implementation of radiation)

Observations with Rayleigh lidar (operated by LATMOS)

Location : Observatoire de Haute Provence (43.9°N, 5.7°E)

Rayleigh lidar (Hauchecorne & Chanin, 1980), is operated continuously during nighttime since 1978, allowing for decadal analyses (e.g. Khaykin et al. 2014 ; Mze et al. 2014)

Altitude range probed : 30-90 km
Vertical resolution : 75 m
Accuracy : < 1 K (below 70 km altitude)

16 nights (4-hourly profiles each) with observations over the DYAMOND (phase II) period. Hourly temperature profiles and hourly perturbation ΔT profiles (assumed to be due to GW) are provided.

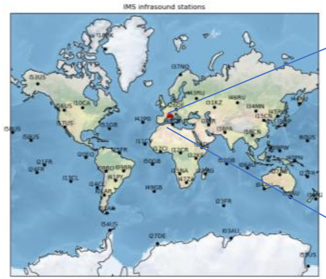

Infrasound propagation simulations using atmospheric fields from high-resolution global models resolving gravity waves

C. Listowski et al.

METHODS

Deriving the vertical gravity wave perturbations

- The total field is considered as the superposition of a background field and a perturbed field caused by GW.
- The modelled outputs are interpolated on a vertical grid with dz=1,5 km
- The model background field is determined by filtering out vertical wavelengths smaller than 15 km (cut-off wavelength *lambda_c*) with a butterworth filter (3rd order). (see e.g. Baumgarten et al., 2017)
- Subtracting the background from the total field gives the perturbed GW field.

ICON/dpp0014

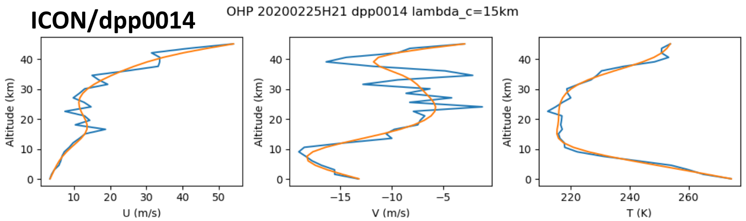

$X - X_{smooth} = \Delta X_{GW}$

for X=U, V, or T

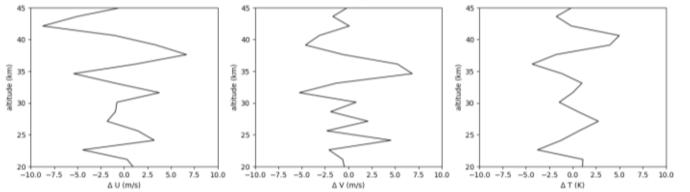

ICON/dpp0015

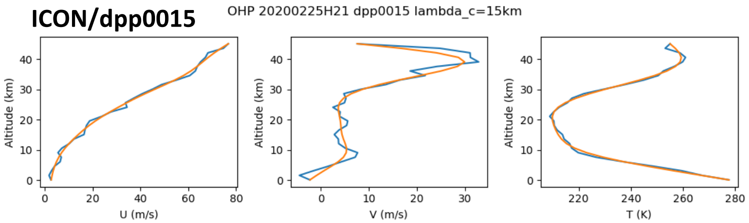

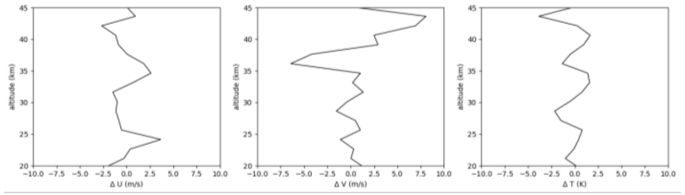

1/ Background fields and GW perturbation fields are compared to the OHP lidar observations
2/ GW-related energies are derived for the various IMS stations

Infrasound propagation simulations using atmospheric fields from high-resolution global models resolving gravity waves

C. Listowski et al.

RESULTS

Comparing the average observed temperature profile to each of the four ICON configuration's average

Modelled mean fields (3-hourly outputs) are averaged across the 16 nights of lidar observations (considering 18h00 and 21h00 UTC).

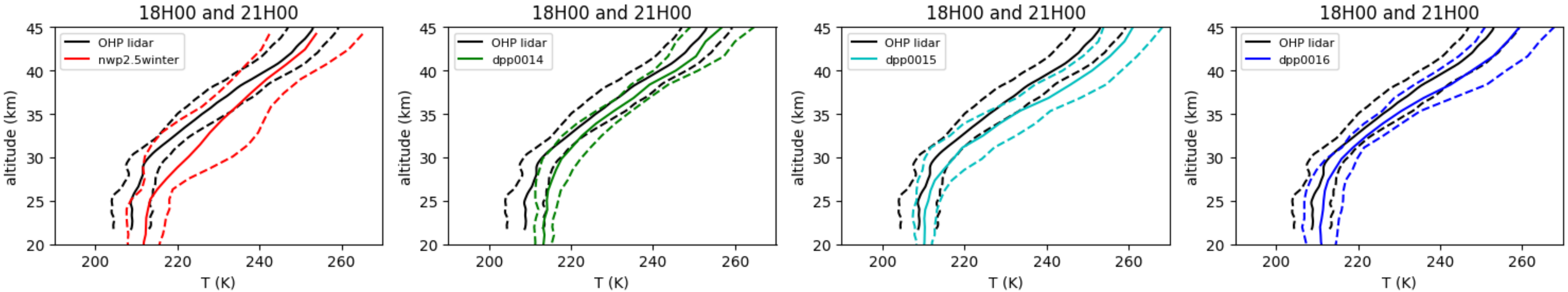

Solid line is the average T profile and dashed lines are +/- the standard deviation.

- The mean field and its average variability across the DYAMOND period are well captured by the model configurations.
- Configuration dpp0014 is closer to observations above 35 km and dpp0015/16 are performing better below 30 km.
- The nwp2.5 configuration gives the least satisfying comparison.

Infrasound propagation simulations using atmospheric fields from high-resolution global models resolving gravity waves

C. Listowski et al.

RESULTS

Comparing the average observed perturbation profile (ΔT) to each of the four ICON configuration's average

Modelled mean |ΔT| fields (3-hourly outputs) obtained as explained on slide 5 are averaged across the 16 nights of lidar observations.

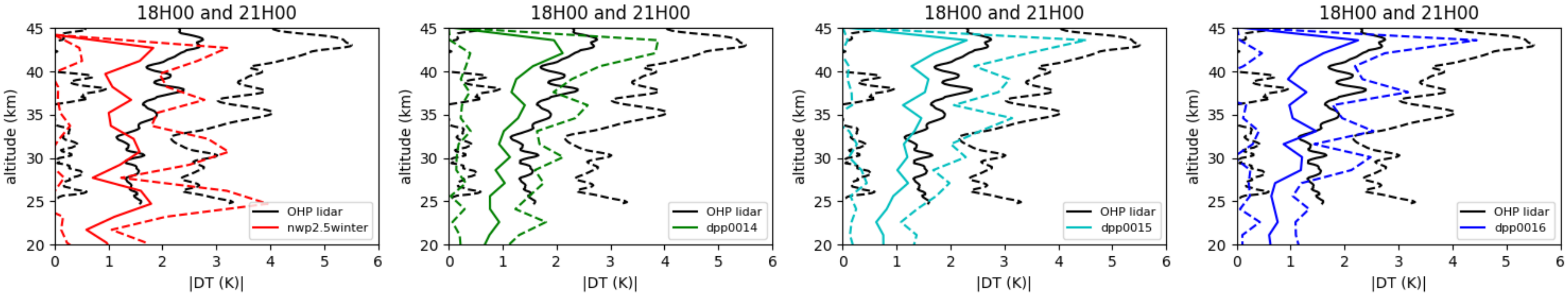

Solid line is the average |ΔT| profile and dashed lines are +/- the standard deviation.

- The average |ΔT| and the range of variability are better captured by the dpp0015 configuration.
- Overall the perturbation amplitudes are well retrieved (except some extreme values) and the nwp configuration performs the least well.

Infrasound propagation simulations using atmospheric fields from high-resolution global models resolving gravity waves

C. Listowski et al.

RESULTS

Examples of single hourly T and ΔT profiles (18H, at selected dates)

- The model mean temperature bias generally increases with time most probably because of the free running mode of the simulations

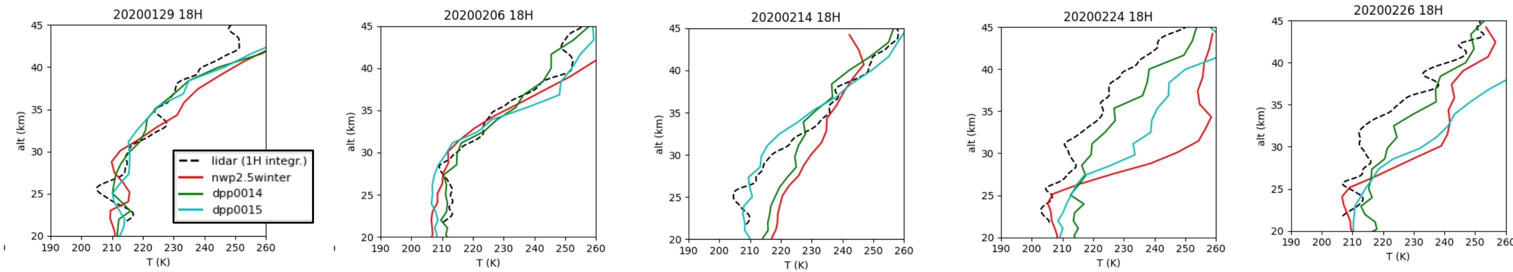

- However, the GW perturbations amplitudes bias do not necessarily increase in the same way.

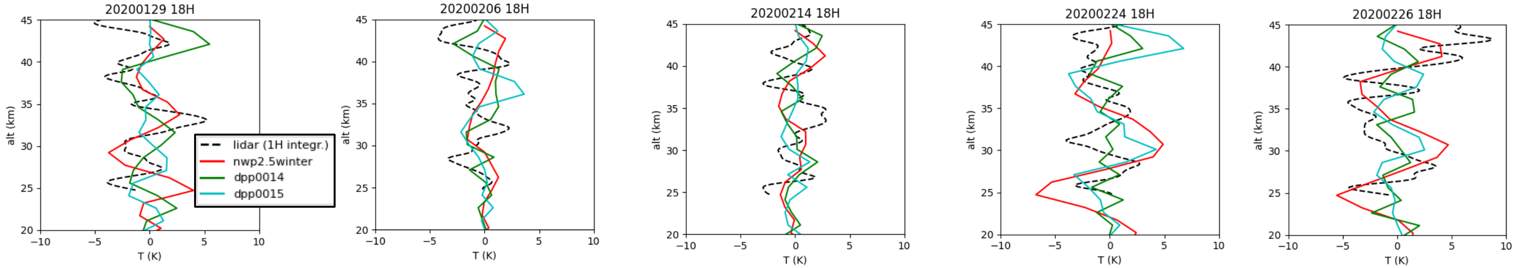

Infrasound propagation simulations using atmospheric fields from high-resolution global models resolving gravity waves

C. Listowski et al.

RESULTS

Temperature power spectral densities (PSD) for observations (dz=75 m) and model outputs (dz=1.5 km).

Vertical spectra as a funtion of $1/\lambda_z$ are derived for each vertical profile and the median and percentiles (33% and 66%) of spectra are derived across the whole period.

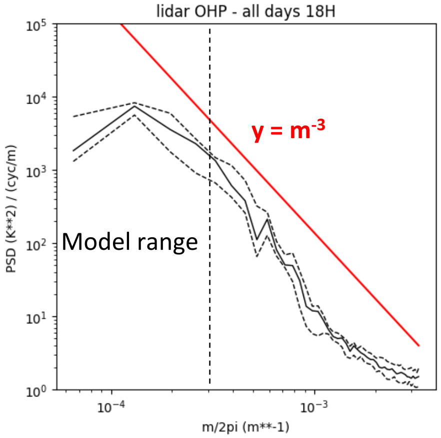

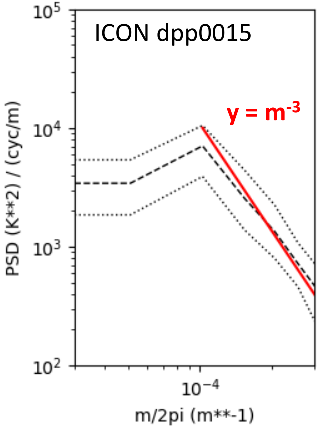

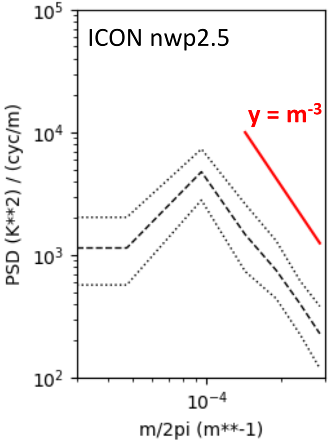

- The characteristic -3 slope for GW vertical spectrum is retrieved in the observations and the model temperature spectra.
- The spectrum of nwp2.5 consistently reaches lower values than dpp0015 (as expected from vertical profiles in the previous slide). The maximum amplitude for dpp0015 simulations is comparable to that of the observations.

Infrasound propagation simulations using atmospheric fields from high-resolution global models resolving gravity waves

C. Listowski et al.

RESULTS

Deriving average potential energy of gravity waves (E_p)

- E_p values are consistent with (winter) climatology at OHP (Khaykin et al. 2014 ; Mze et al. 2014) with $1 < E_p < 10$ J/kg between 20 and 40 km altitude
- This is consistent with the comparable PSDs (obs. vs. model) shown in the previous slide 9.

$$E_p = \frac{1}{2}\left(\frac{g}{N}\right)^2\left(\frac{\Delta T}{\bar{T}}\right)^2$$

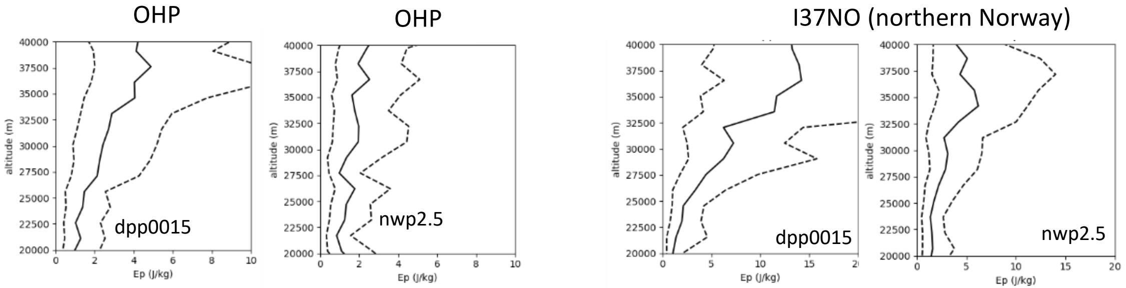

Latitudinal variation of average E_p(20-40 km) at IMS stations over 20jan-29Feb 2020 :

- Largest values in the tropics (convection ?)
- Lowest values in the mid/high southern latitudes (effect of wind tropo/strato inversion in this season, which filters GW coming from orography in the southern hemisphere ?)

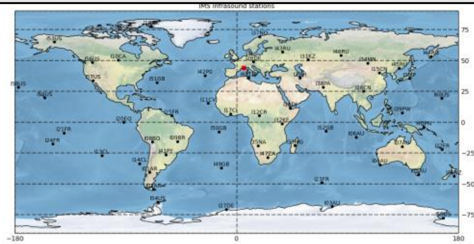

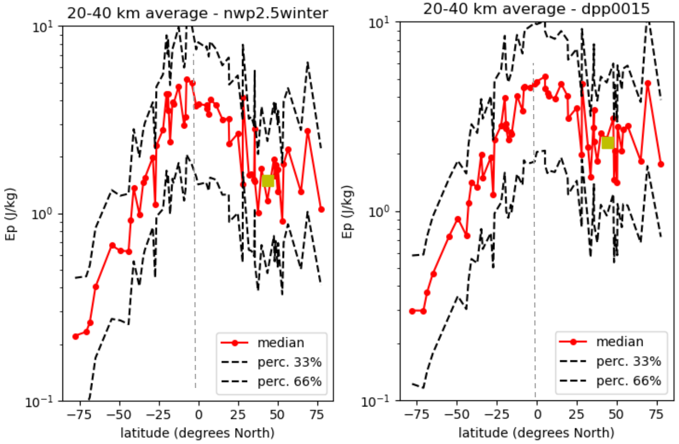

- Similar pattern of Ep vs. Lat for all model configurations.
- EP(dpp0015)/Ep(nwp2.5) = 1.25-2 (except around the equator ~1)

One question is :can we see an impact on infrasound propagation characteristics, which relates to the trend (left figure), and – on a differente note - to the above difference between both configurations.

Infrasound propagation simulations using atmospheric fields from high-resolution global models resolving gravity waves

C. Listowski et al.

RESULTS

Infrasound guiding : large-scale or GW effect ? (discussion 1/2 ; work in progress)

- Different model configurations result in different guiding with variable turning altitude (z_t) for acoustic rays (where $C_{eff}(z=z_t)/C_{eff}(z=0)>1$).

*Example of C_{eff} ratio profiles at **OHP station** 20 Jan 2020 until 29 Feb 2020, from model outputs, for two directions (North/East-ward)*

$$C_{eff} = \mathbf{C} + \vec{n} \cdot \vec{U},$$

where $\vec{n}$ is the direction of propagation and $\vec{U}$ the wind speed vector.

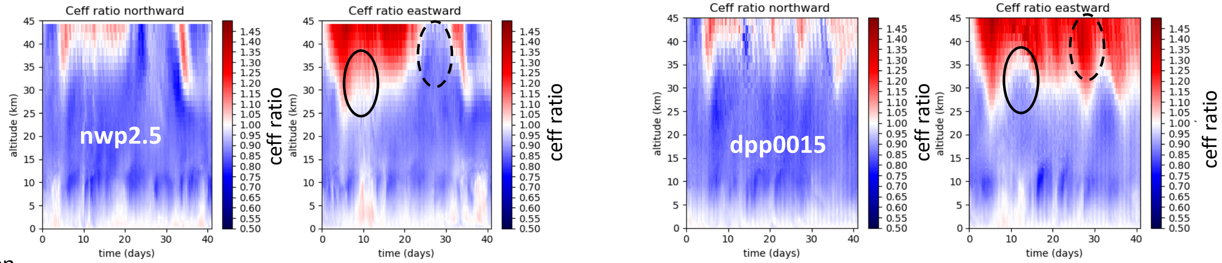

→ Effect of the mean field differences on stratospheric guide (little effect of GW on IS guiding at these times)

- The average gravity wave energy may be largest at some station (e.g. I20EQ, see previous slide), but the stratospheric guide (large-scale effect) far from IS reflexion conditions, so that GW will not force some turning height (see below). Conversely, it may be critical to guiding (black circle)

Station I20EQ (Ecuador)
(25 Feb 2020, 18H00)

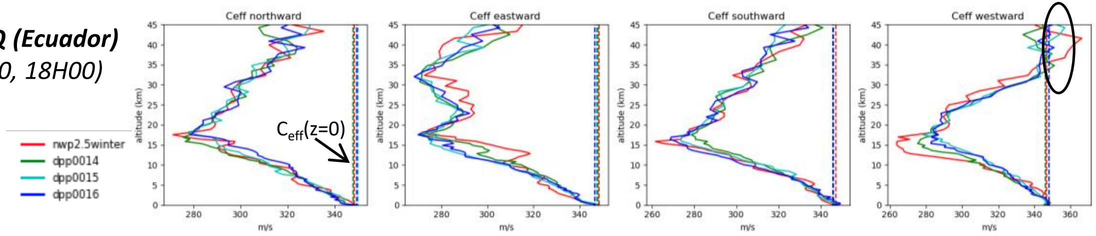

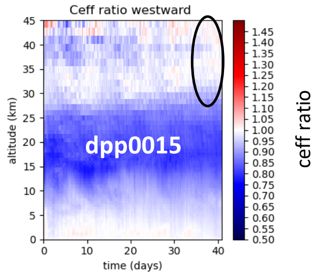

Infrasound propagation simulations using atmospheric fields from high-resolution global models resolving gravity waves

C. Listowski et al.

Infrasound guiding : large-scale or GW effect ? (discussion 2/2 ; work in progress)

RESULTS

Station I48TN (Tunisia)
(31 Jan 2020, 18H00)

GW allowing northward guiding for dpp0015 and southward guiding for dpp0016

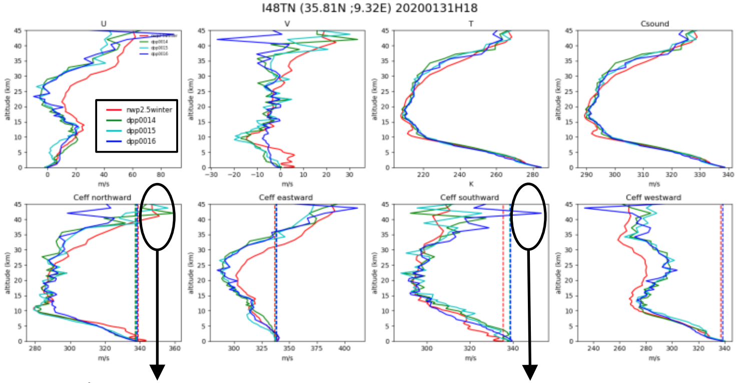

dpp0015 – AZI=0°

dpp0016 – AZI=180°

Ray tracing tool documented in Garces et al. 1998 (tau-p method)

50 ray parameters between $1/vt_{min}$ and $1/vt_{max}$ with vt_{min}/vt_{max} = 320/500 m/s)

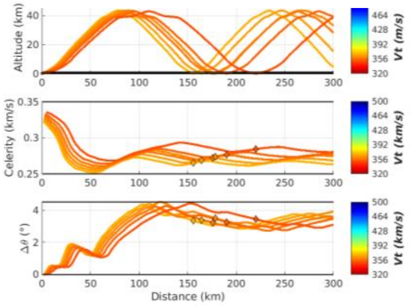

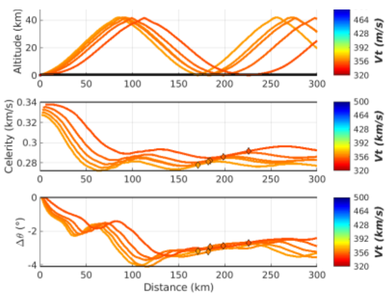

Plan :

Performing propagation simulation on the background profile (with GW filtered out) and with the total profile (including GW).

Quantifying the difference between both scenarios in terms of infrasound propagation characteristics (guiding or not, value for z_t, $\Delta\theta$, X_{IS1}).

Quantifying the impact of GW at various IMS locations on IS guiding and discuss with relation to global GW energy distribution.

Assessing how critical GWs are (with relation to large-scale effect) in impacting IS guiding at IMS or national station locations, regionally.

Infrasound propagation simulations using atmospheric fields from high-resolution global models resolving gravity waves

C. Listowski et al.

CONCLUSIONS

Conclusions :

- We use the ICON model's DYAMOND initiative's outputs (Phase II, 20 jan – 29 Feb 2020) to investigate GW properties at infrasound stations.
- We present first DYAMOND/lidar comparisons in the stratosphere in terms of mean field and GW perturbations (profiles and spectra) and demonstrate the overall good performance of the simulations, also in terms of GW perturbations, at Observatoire de Haute Provence.
- We derive potentiel energy of GW at OHP and IMS stations and show the latitudinal distribution of E_p averaged between 20 and 45 km.
- We discuss a way to investigate links between the variability in GW activity (energy) and the GW effect on IS guiding and propagation through the IMS network, with respect to large-scale effects.

Perspective :

- Perform propagation simulation on GW-filtered/unfiltered atmospheric profiles and assess GW effect. Compare to large-scale effects.
- Use DYAMOND phase I outputs (August 2016) to compare with the winter phase II outputs where stratospheric jets are reversed.
- Assess the impact on the detection capability of the IMS (see Le Pichon et al. 2019).
- Add other models that are part of the DYAMOND initiative. This may give an « ensemble » picture of the impact of GW.

Infrasound propagation simulations using atmospheric fields from high-resolution global models resolving gravity waves

C. Listowski et al.

REFERENCES

References :

- Baumgarten, K., M. Gerding, and F.-J. Lübken (2017), Seasonal variation of gravity wave parameters using different filter methods with daylight lidar measurements at midlatitudes, *J. Geophys. Res. Atmos.*, *122*, 2683–2695, doi:10.1002/2016JD025916.
- Bölöni, G., Kim, Y., Borchert, S., & Achatz, U. (2021). Toward Transient Subgrid-Scale Gravity Wave Representation in Atmospheric Models. Part I: Propagation Model Including Nondissipative Wave–Mean-Flow Interactions, Journal of the Atmospheric Sciences, 78(4), 1317-1338.
- Chunchuzov, I., & Kulichkov, S. (2019). Internal gravity wave perturbations and their impacts on infrasound propagation in the atmosphere. In *Infrasound Monitoring for Atmospheric Studies* (pp. 551-590). Springer, Cham.
- Cugnet, A. De La Camara, F. Lott, C. Millet, B. Ribstein, (2018), « Non-orographic gravity waves : representation in climate models and effects on infrasound », dans A. Le Pichon, É. Blanc, A. Hauchecorne, Infrasound monitoring for atmospheric studies, Springer, New York, p. 827-844.
- de la Camara, F. Lott, « A parameterization of gravity waves emitted by fronts and jets », Geophys. Res. Lett., 42, p. 2071-2078 (2015).
- Drob, D. P., D. Broutman, M. A. Hedlin, N. W. Winslow, and R. G. Gibson (2013), A method for specifying atmospheric gravity wavefields for long-range infrasound propagation calculations, J. Geophys. Res. Atmos., 118, 3933–3943,
- Fritts, D. C., and Alexander, M. J. (2003), Gravity wave dynamics and effects in the middle atmosphere, *Rev. Geophys.*, 41, 1003.
- Gardner, C. S., C. A. Hostetler, and S. J. Franke (1993), Gravity wave models for the horizontal wave number spectra of atmospheric velocity and density fluctuations, J. Geophys. Res., 98, 1035-1049
- Garcés Milton A. , Roger A. Hansen, Kent G. Lindquist, Traveltimes for infrasonic waves propagating in a stratified atmosphere, Geophysical Journal International, Volume 135, Issue 1, October 1998, Pages 255–263, https://doi.org/10.1046/j.1365-246X.1998.00618.x
- Hauchecorne, A., and M. L. Chanin (1980), Density and temperature profiles obtained by lidar between 35 and 70 km, Geophys. Res. Lett., 7(8), 565–568, doi:10.1029/GL007i008p00565.
- Hedlin, M. A. H., and D. P. Drob (2014), Statistical characterization of atmo- spheric gravity waves by seismoacoustic observations, J. Geophys. Res. Atmos., 119, 5345–5363
- Khaykin, S. M., A. Hauchecorne, N. Mzé, and P. Keckhut (2015), Seasonal variation of gravity wave activity at midlatitudes from 7 years of COSMIC GPS and Rayleigh lidar temperature observations, Geophys. Res. Lett., 42, 1251–1258, doi:10.1002/2014GL062891.
- Kim, Y., Bölöni, G., Borchert, S., Chun, H., & Achatz, U. (2021). Toward Transient Subgrid-Scale Gravity Wave Representation in Atmospheric Models. Part II: Wave Intermittency Simulated with Convective Sources, Journal of the Atmospheric Sciences, 78(4), 1339-1357
- Le Pichon, A., Ceranna, L., Vergoz, J., & Tailpied, D. (2019). Modeling the detection capability of the global IMS infrasound network. In *Infrasound Monitoring for Atmospheric Studies* (pp. 593-604). Springer, Cham
- Mzé, N., A. Hauchecorne, P. Keckhut, and M. Thétis (2014), Vertical distribution of gravity wave potential energy from long-term Rayleigh lidar data at a northern middle-latitude site, J. Geophys. Res. Atmos., 119, 12,069–12,083, doi:10.1002/2014JD022035.
- Stephan, C. C., Strube, C., Klocke, D., Ern, M., Hoffmann, L., Preusse, P., & Schmidt, H. (2019). Intercomparison of gravity waves in global convection-permitting models. Journal of the Atmospheric Sciences, 76(9), 2739-2759.
- Stephan, C. C., Strube, C., Klocke, D., Ern, M., Hoffmann, L., Preusse, P., & Schmidt, H. (2019). Gravity waves in global high-resolution simulations with explicit and parameterized convection. Journal of Geophysical Research: Atmospheres, 124, 4446–4459.
- Stevens, B., Satoh, M., Auger, L., Biercamp, J., Bretherton, C. S., Chen, X., ... & Kodama, C. (2019). DYAMOND: The DYnamics of the atmospheric general circulation modeled on non-hydrostati domains. Progress in Earth and Planetary Science, 6(1), 61.
- Vallage et al. (2021) Multitechnology characterization of an unusual surface rupturing intraplate earthquake: the ML 5.4 2019 Le Teil event in France, Geophysical Journal International, Volume 226, Issue 2, August 2021, Pages 803–813
- Zängl, G., D. Reinert, P. Ripodas, and M. Baldauf (2015): The ICON (icosahedral non-hydrostatic) modelling framework of DWD and MPI-M: Description of the non-hydrostatic dynamical core. Quart. J. Roy. Meteor. Soc., 141, 563–579